nature physics

SUPPLEMENTARY INFORMATION

DOI: 10.1038/NPHYS1479

"Back-action Evading Measurements of Nanomechanical Motion"

J. Hertzberg, T. Ndukum, T. Rocheleau, M.Savva, A.Clerk, K.C. Schwab

Supplementary Information

The devices described in this paper consist of a nanomechanical resonator (NR) coupled to a superconducting microwave resonator (SR).

Device parameters

Direct measurement of RF behavior:

$\omega_{sr} = 2\pi \cdot 5.00684$ GHz	SR resonant frequency
$\kappa = 2\pi \cdot 494$ kHz	SR damping rate
$\omega_{nr} = 2\pi \cdot 5.5717$ MHz	NR resonant frequency (varies up to 50 Hz with temperature and random drift)

Fabrication geometry, verified by inspection in SEM:

w = 16 μm	Width of Al centerline of SR
d_{sr} = 10 μm	Gap between SR centerline and ground plane
t = 260 nm	Thickness of Al film on SR
l = 30 μm	length of mechanical resonator
l_g = 26 μm	length of capacitive gate opposite resonator
w = 170 nm	width of mechanical resonator
t_{SiN} = 60 nm	thickness of SiN

DOI: 10.1038/NPHYS1479

$t_{Al} = 105$ nm	thickness of Al film on NR
d = 85 nm	Distance between the NR and gate

Calculated from the geometry:

$m = (2.2 \pm 0.3)\cdot 10^{-15}$ kg	effective mass of NR
$k = 2.70 \pm 0.37$ N/m	spring constant of NR
$Z_0' = 50\ \Omega$	Characteristic impedance of SR waveguide forming SR (defined by w, d_{sr} and dielectric constant of substrate)
$x_{zp} = \sqrt{\hbar/2m\omega_m} = 26 \pm 2$ fm	zero-point motion of the NR

Parameters derived from RF measurement (see sections 5, 6 and 9):

C = 1.0 pF	Effective SR capacitance
L = 1.0 nH	Effective SR inductance
$C_K = 4.38 \pm 0.84$ fF	Coupling capacitance into and out of SR
$\partial C / \partial x = 3.0 \pm 0.6$ aF/nm	Change in capacitance for displacements
$\partial \omega_{sr} / \partial x = 2\pi\cdot (7.5 \pm 1.6$ kHz/nm)	Coupling constant
$C_g = 253 \pm 54$ aF	Capacitance between the NR and SR
$\partial^2 C / \partial x^2 = 0.06$ F/m^2	Second derivative of capacitance
$\lambda = \frac{\omega_{sr}}{2C}\frac{\partial^2 C_g}{\partial x^2} = 2\pi \cdot 0.15$ kHz/nm^2	Nonlinear coupling constant

1) Measurement Circuit

Figures SI-01 to SI-03 show the details of our measurement circuit. Wiring within the fridge is fixed, whereas the wiring outside the fridge was reconfigured for the several different kinds of measurements.

Within the fridge, on the drive line, microwave frequency blackbody radiation is carefully managed using cold NiCr attenuators (Midwest Microwave). Microwave signal lines between 300K and 4K are Au-plated/CuNi-inner, CuNi-outer, 50Ω semirigid 0.085" diameter coax cables (Coax Co, Ltd, Japan). At stages below 100 mK on the drive line, and between the mixing stage and 1.5 K on our return line, microwave signals are carried by Nb-inner, Nb-outer 50Ω semi-rigid 0.085" coax cables (Coax Co, Ltd, Japan). Segments of superconducting Al microstrip on silicon thermalize the inner conductor of the microwave lines. On the return line, measured signals are amplified by a cryogenic HEMT amplifier (CITCRYO1-12A, S. Weinreb, Caltech) which has a noise temperature of 3.56 +/-1K at 5 GHz. This amplifier is anchored to 4K and is isolated from the sample by two cryogenic circulators functioning as isolators (Quinstar QCY-050100CM0). A third coaxial line carries low-frequency (< 10 MHz) signals for driving the mechanical resonator. This wiring is CuNi-inner, CuNi-outer 0.012" diameter cable (Coax Co, Ltd, Japan) and has about 18 dB of attenuation at 5.5 MHz. Signal from this line is applied to the device via a bias-tee (Anritsu K252) mounted at the mixing stage. On this line, Cu powder filters at the 1.5K and mixing stages provide isolation of high frequencies.

DOI: 10.1038/NPHYS1479

Design and performance of powder filters and stripline thermalizers are described in the PhD dissertation by M. LaHaye. [**1**]

All sources and measurement devices are synchronized to a single 10MHz source derived from an SRS FS725 rubidium standard. Microwave sources 1 and 2 are Agilent E8257D; source 3 is a Rohde and Schwarz SMA100A. The MHz-range RF source was a Tektronix AFG3252. The power-splitters are Pasternack model PE2028; directional couplers are Pasternack model PE-2204-10 and PE-2210-20. The room temperature low noise amplifier is a Miteq AFS3-04700530-07-8P-4-GW. The bandpass filter is a Minicircuits VBFZ-5500. The IQ mixer is a Marki Microwave IQ0307LXP. The first two noise generating amplifiers are Quinstar OLJ-04122025-J0. The third is a Miteq LCA-0408. The room temperature circulator is a Ditom D3C-4080. Finally, the diode detector was an Eclipse DT4752A3.

Our microwave sources produce phase and amplitude noise totaling -145dBc/Hz at an offset 5.5 MHz from the carrier. Given the pump strengths used in this experiment, this phase noise will excite the SR out of its ground state and into a thermal state. We suppress this noise using TE_{011} cavity filters, following a design described in ref **[2]** and ref **[3]**. The cavities are each cooled to 77K to improve the quality factor, by mounting in a sealed probe filled with He gas and immersed in liquid nitrogen. The frequency of each cavity may be tuned in situ. At an offset of 5.57 MHz from the carrier, we obtain a filtering factor greater than 50dB. This results in phase noise of ~-195 dBc/Hz. When the maximum microwave pump power of +25dBm is applied, and then attenuated by ~44dB

within the fridge (see measurement schematic), the phase noise at the input of the device should be far below the level of quantum vacuum fluctuations (~ -205 dBm/Hz). Further details appear in reference **[4]**.

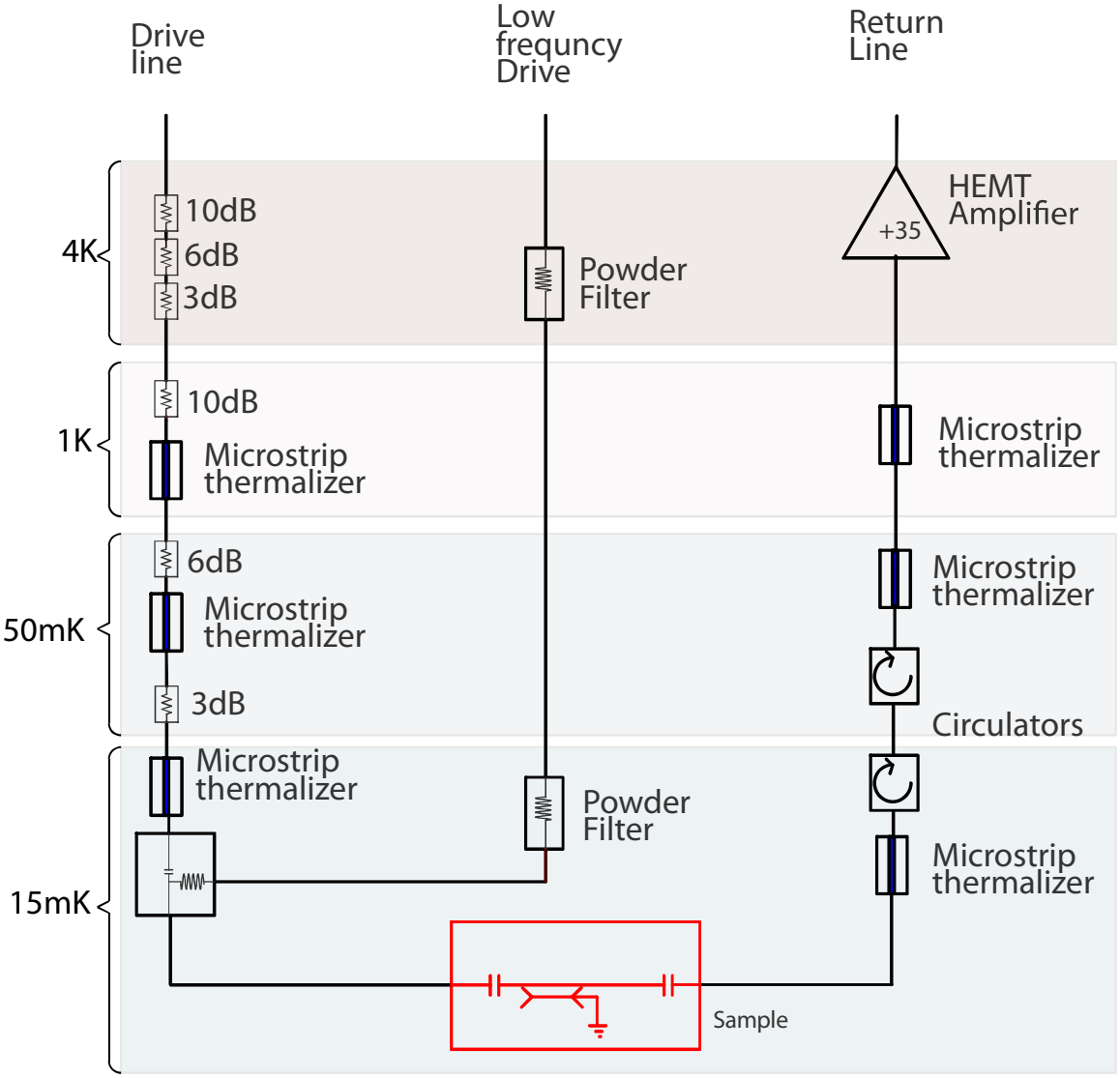

Figure SI-01. Schematic of interior wiring within dilution fridge.

DOI: 10.1038/NPHYS1479

Care was taken to limit spurious signals and interference. The dilution fridge and instrumentation were installed in a shielded room. RF signal lines into and out of the shielded room were routed through DC-block filters. All instrumentation amplifiers were powered from batteries. Of the RF electronics, only the two Agilent microwave sources and one SR844 lock-in were operated inside the shielded room, because cable attenuations limited the power that could be supplied to the fridge from outside the shielded room. The microwave pump signals passed through DC-block filters before entering the fridge.

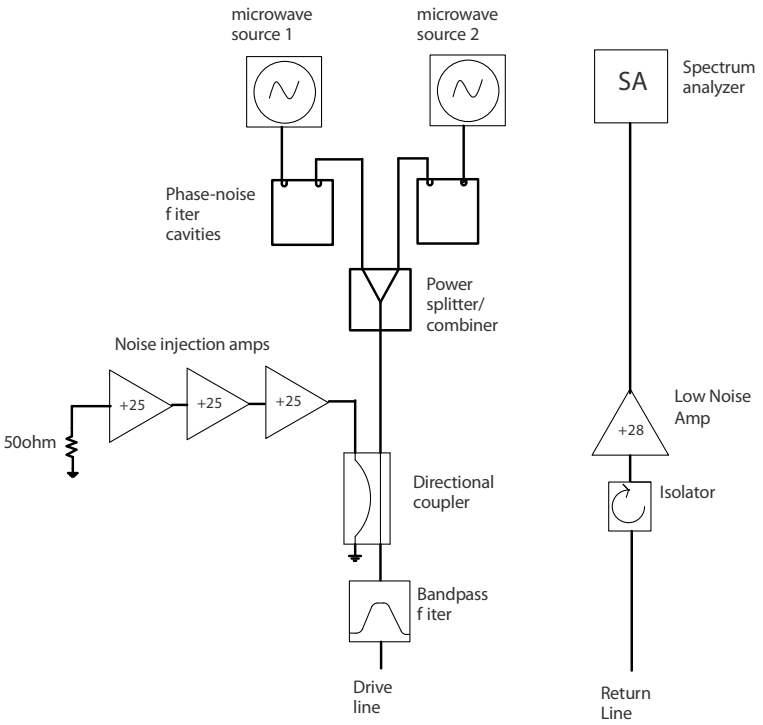

Figure SI-02. Schematic for BAE demonstration or backaction cooling. When cooling, noise-injecting amplifiers were shut off. Drive and return lines join to corresponding points on fridge.

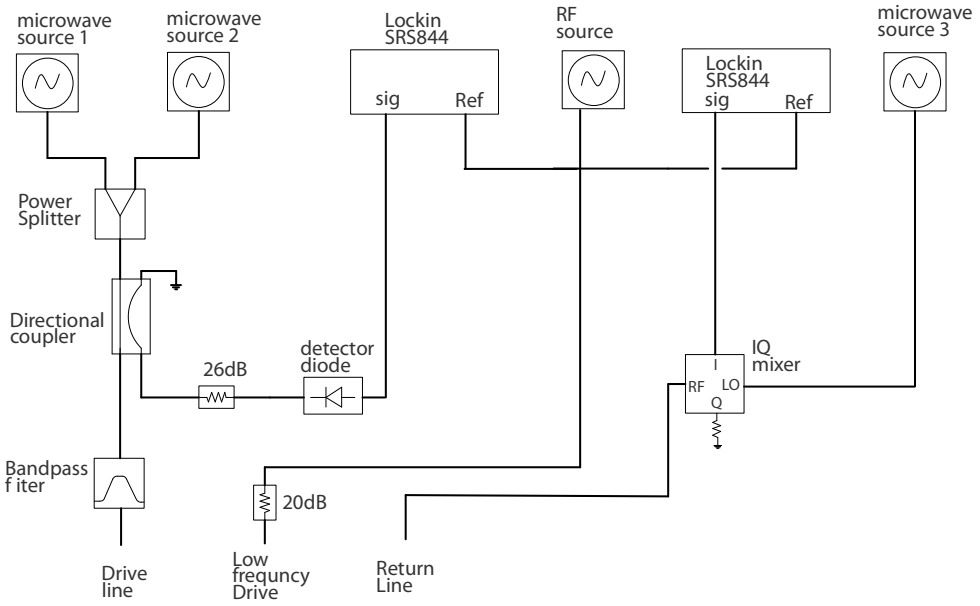

Figure SI-03. Schematic for demonstrating single-quadrature detection of driven NR. Signal lines join to corresponding points on fridge.

2) Superconducting Microwave Resonator (SR)

The superconducting microwave resonator (SR) consists of a half-wave segment of superconducting aluminum coplanar waveguide (CPW) having a fundamental resonance of about 5 GHz [**5**]. The characteristic impedance of the CPW was designed to be 50 ohms. Coupling capacitors C_K define the ends of the half-wave segment and permit microwave energy to be coupled into and out of the SR. At the power levels employed in this paper the quality factor of the SR was approximately 1.014×10^4, corresponding to a

DOI: 10.1038/NPHYS1479

linewidth of 494 kHz. At power levels corresponding to more than ~$2.5 \cdot 10^8$ pump photons in the SR, the device exhibited strong internal dissipation and thermal heating. This set an upper practical limit on the pump power that could be applied during measurement.

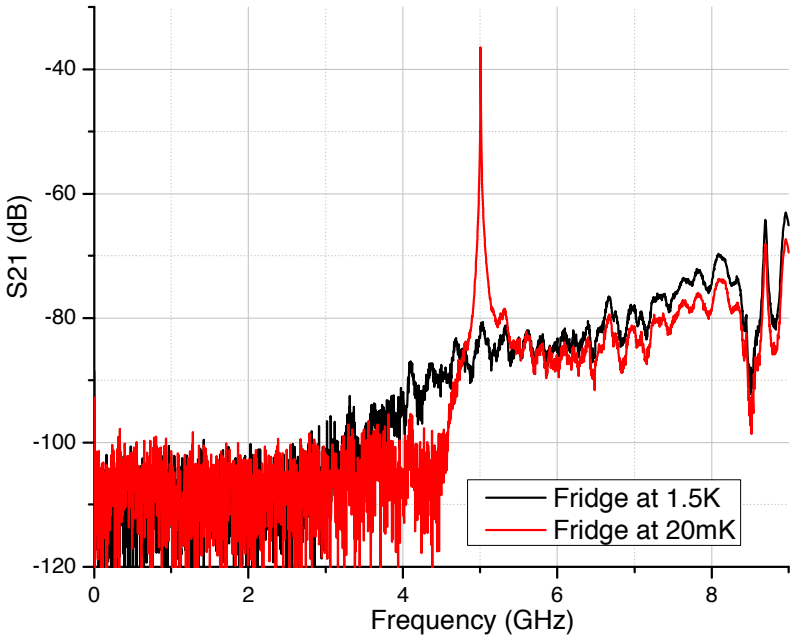

Figure SI-04. Wide span transmission spectrum of SR. Superconducting 5 GHz resonance vanishes in normal (1.5K) SR.

Noise radiating from the amplifier input was prevented from exciting the SR by two cryogenic circulators separating the HEMT amp from the sample (see fig SI-01). With no pump power applied, we observed no SR resonance in the emitted spectrum, after averaging the output signal for a duration sufficient to resolve an emitted power

corresponding to less than 1 quantum stored in the SR. From this we conclude that amplifier noise did not excite the SR above its ground state.

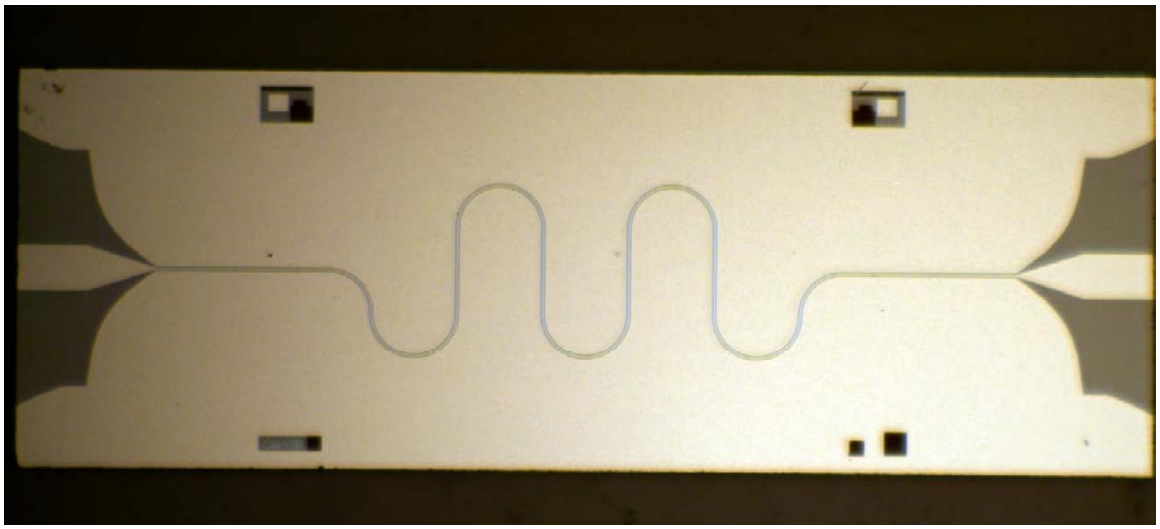

Figure SI-05. 3.5mm × 10mm chip with coplanar waveguide forming SR. Coupling capacitors C_K are barely visible in straight regions on either end of meander section.

3) Device Fabrication

Our device fabrication begins with virgin, ultra-high resistivity Si wafers: <100> orientation, 500 micrometers thick, with resistivity > 10 kΩ·cm. The wafers are coated with 70nm thick high-stress, low pressure chemical vapor deposited (LPCVD) silicon nitride (SiN), which will form the structural material of the nano-resonator. Because we have found the nitride to be a lossy dielectric at microwave frequencies, before further

DOI: 10.1038/NPHYS1479

fabrication the nitride is first stripped from the wafer in all places except for 2μm × 37μm "patches" where the nano-resonators are to be located. This is done using photolithographic patterning and plasma etching (150W, 60mTorr, 50sccm CHF_3/5 sccm O_2) followed by a smoothing buffered oxide (BOE) wet etch. We use BOE (6:1) which etches the nitride at ~5-10Å/min.

Next, the superconducting microwave resonator (SR) is formed. This is done using standard photolithography and lift-off of thermally evaporated Al (99.999% pure). Next, the NR is defined using electron beam lithography and lift-off of electron-beam evaporated Al on top of the SiN patches. The NR is released from the substrate using two consecutive plasma etches, one to vertically etch the SiN (150W, 60mTorr, 50sccm CHF_3/5 sccm O_2) and the second to isotropically remove the silicon (100W, 125mTorr, 50 sccm SF_6) underneath the NR, thus leaving a structure formed of 60 nm of SiN coated with 105 nm of Al. Two nanoresonators were fabricated onto the chip, both of which were coupled to the SR, but only one is studied in this paper. The fabrication was performed at the Cornell Nanoscale Fabrication facility.

The final chip is 3.5mm × 10mm × 500 μm and is mounted directly onto a gold-plated copper surface of the sample package. Coplanar wave guides which feed the pump signal into the chip and carry the signals out are fabricated onto copper-plated high dielectric-constant circuit board (Arlon AR1000, 0.015" thick, $\varepsilon = 10$). Figures SI-06 and SI-07 show the mounted sample. To ensure proper grounding of the SR groundplane, a large

number of Al wirebonds are used to connect the Al groundplane of the chip to the groundplane of the circuit board as well as to connect the two halves of the groundplane.

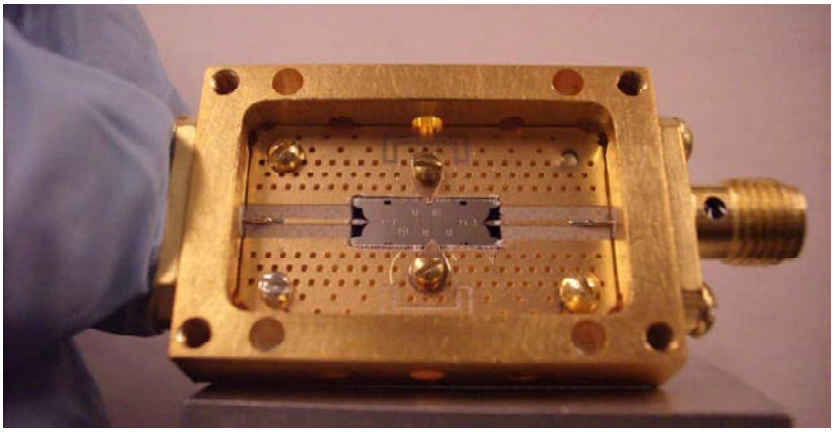

Figure SI-06. Chip in gold-plated copper sample box with RF leads.

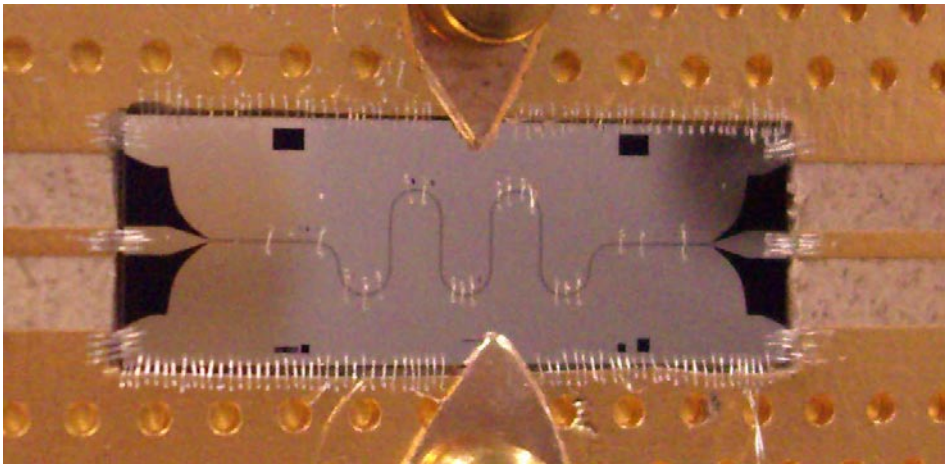

Figure SI-07. Close up of chip in sample box showing wirebonds.

DOI: 10.1038/NPHYS1479

4) Equivalent Circuit Model

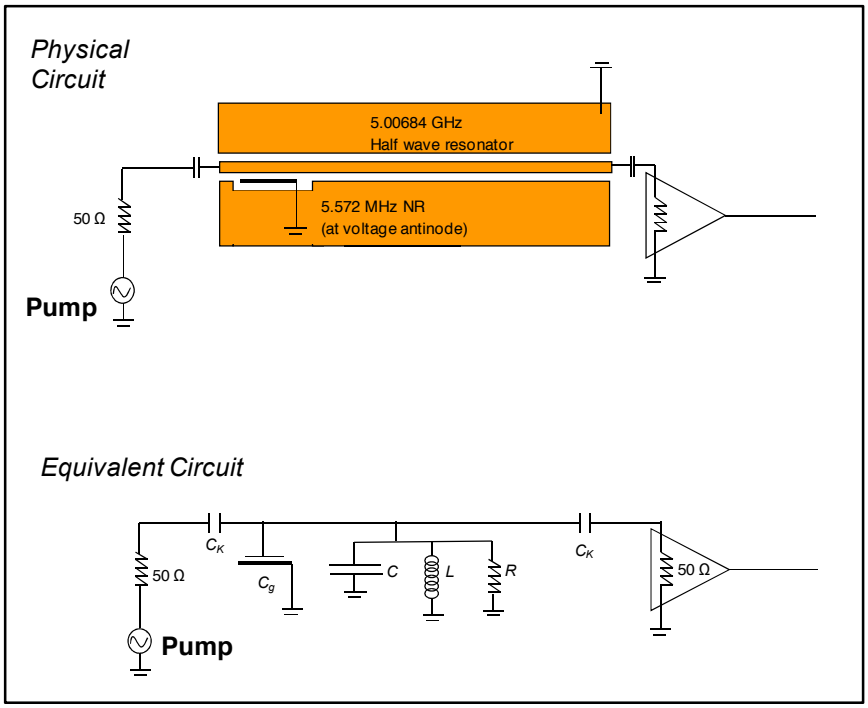

Figure SI-08. Device schematic and equivalent circuit.

The SR behaves as a microwave cavity which is probed via transmission. It may be modeled by a lumped-element LRC circuit in parallel with coupling capacitors C_K and the 50 ohm impedance of attenuators and amplifier (figure SI-08), which impose additional dissipation. We use an analysis similar to that found in Ref **[5, 6].**

The total capacitance of the equivalent circuit is $C_T = C + 2C_K + C_g$. The CPW transmission line forming the SR was engineered to have a characteristic impedance of

$Z_0' = 50\ \Omega$. For the equivalent circuit model, the characteristic impedance Z_0 and total capacitance C_T may be found as follows:

$$Z_0 = \frac{2}{\pi} \cdot Z_0' \qquad C_T = \frac{1}{\omega_{sr} Z_0} \tag{1}$$

Because in our devices, $C >> C_K >> C_g$, we will approximate $C_T = C$ wherever necessary for simplicity of notation.

As shown in figure SI-01, power applied to the drive line is reduced by the attenuators and other components before reaching the SR ("loss"), and signals emerging from by the SR are amplified before being detected in the return line ("gain"). Thus the power transmitted by the system at a pump frequency ω is found to be

$$P_{out} = P_{in} \cdot loss \cdot \frac{\kappa_{ext}^2}{\kappa^2 + 4(\omega - \omega_{sr})^2} \cdot gain \tag{2}$$

where κ_{ext} is the loading of the SR via the coupling capacitors to the 50-ohm environment, $\kappa_{ext} = (4/\pi)\omega_{sr}(\omega_{sr} C_K)^2 \cdot 50\Omega \cdot Z_0'$. The loading at each end of the SR contributes half of κ_{ext}.

Following the theory of backaction cooling presented in **[14]**, we expect the backaction damping rate to be proportional to the number of microwave pump quanta $\bar{n}_p$ stored in the SR. To compute $\bar{n}_p$, we first find from the equivalent circuit model the stored energy

DOI: 10.1038/NPHYS1479

in the SR, $E_{sr} = \frac{1}{2}CV^2$, where V is the peak amplitude of the voltage oscillating at frequency ω in the SR. Then $\bar{n}_p = E_{sr}/\hbar\omega$ may be found from either the input or output power of the system, if the line-loss and/or gain are known:

$$\begin{aligned}\bar{n}_p &= \frac{1}{\hbar\omega}\cdot P_{in}\cdot loss\cdot\frac{2}{\kappa_{ext}}\cdot\frac{\kappa_{ext}^2}{\kappa^2+4(\omega-\omega_{sr})^2}\\ &= \frac{1}{\hbar\omega}\cdot\frac{2}{\kappa_{ext}}\cdot P_{out}/gain\end{aligned} \qquad (3)$$

5) Calibration of Mechanical Mode Temperature

Referring again to the circuit model, we see that motion of the mechanical resonator modulates the capacitance C_g(x). This adds to the equations for the voltage in the SR a term $\partial C_g/\partial x\cdot V(t)\cdot x(t)$, where $x(t) = x_0\cos(\omega_m t)$, thereby coupling the mechanical motion to the electromagnetic field. For a pump oscillating at frequency ω, the product of $V(t)$ and $x(t)$ leads to sidebands at frequencies $\omega \pm \omega_m$. Choosing $\omega = \omega_{sr} \pm \omega_m$, the sideband of interest falls at frequency ω_{sr}. Solving for the measured sideband power at this frequency yields

$$\begin{aligned}P_{sideb} &= P_{in}\cdot loss\cdot\frac{\kappa_{ext}^2}{\kappa^2+4(\omega-\omega_{sr})^2}\left(\frac{1}{2C}\frac{\partial C_g}{\partial x}Q\right)^2\cdot 2\langle x^2\rangle\cdot gain\\ &= P_{in}\cdot loss\cdot\frac{\kappa_{ext}^2}{\kappa^2+4(\omega-\omega_{sr})^2}\left(\frac{\partial\omega_{sr}}{\partial x}\frac{1}{\kappa}\right)^2\cdot 2\langle x^2\rangle\cdot gain\end{aligned} \qquad (4)$$

Where $\langle x^2 \rangle$ is the RMS amplitude of the NR motion. It is clear from equations (4) and (2) that either P_{sideb}/P_{out} or P_{sideb}/P_{in} is a direct measure of the mechanical amplitude. Although the values of *loss*, *gain*, κ_{ext}, $\partial\omega_{sr}/\partial x$, $\partial C_g/\partial x$ and C are not known a priori to good precision, we may exploit the equipartition theorem to obtain a precise calibration of the *mode temperature* of the mechanical motion, T_{nr}. This technique has been discussed extensively elsewhere in references **[1, 7, 8].** From this we can derive the mechanical amplitude using an estimate of the NR spring constant $k = m\omega_m^2$, where m is the effective mass of the NR. To estimate the effective mass, the total mass is estimated from the known dimensions and densities of the materials in the NR, then multiplied by 0.97 to account for the mode shape and the proportion of the beam length occupied by C_g.

Assuming a single-sided power spectral density, we expect (and observe) the power spectrum of thermal motion of the NR to be $S_x^{NR}(\omega) = \frac{4k_B T_m \omega_m}{mQ_m} \frac{1}{\left(\omega^2 - \omega_m^2\right)^2 + \left(\omega\omega_m/Q_m\right)^2}$, the integral of which gives $\int_0^\infty S_x^{NR}(\omega)\, d\omega/2\pi = \langle x^2 \rangle = k_B T_m/k$. Thus comparing equations (2) and (4) we expect (accounting for small differences between the gain at ω_{pump} and the gain at ω_{sr})

$$\begin{aligned} P_{sideb}/P_{out} &= \left[\left(\frac{\partial\omega_{sr}}{\partial x}\frac{1}{\kappa}\right)^2 \cdot 2\frac{k_B}{k}\right] T_m \\ P_{sideb}/P_{in} &= \left[\left(\frac{\partial\omega_{sr}}{\partial x}\frac{1}{\kappa}\right)^2 \cdot loss \cdot \frac{\kappa_{ext}^2}{\kappa^2 + 4(\omega - \omega_{sr})^2} \cdot gain \cdot 2\frac{k_B}{k}\right] T_m \end{aligned} \qquad (5)$$

DOI: 10.1038/NPHYS1479

A typical measured sideband appears in fig SI-10, with a fit to a Lorentzian. From the fit we extract P_{sideb} (the total area of the Lorentzian), as well as the mechanical frequency ω_m, linewidth $\Gamma_{tot}/2\pi$ and background noise power density S_{bgd}. The level of S_{bgd} is due to amplifier noise and excitation of the SR, which may be driven by phase noise of the microwave source, thermal excitation of the SR, or noise deliberately injected to study back-action evasion.

Figure SI-09 shows P_{sideb}/P_{out}, plotted against fridge temperature, using all of the pump configurations employed with that device (except for single-pump, blue detuned.) We expect the NR to be coupled to both an equilibrium bath (whose temperature is the fridge temperature), as well as an effective bath formed by the SR backaction. In the measurements shown in fig SI-09 the backaction may be neglected because the SR was not excited and the single red-detuned pump was weak enough to neglect backaction cooling. However, at fridge temperatures below ~60mK, the NR appears to be strongly coupled to a third and unidentified dissipative bath whose properties vary on a time-scale of seconds. The dissipation in this bath causes the NR quality factor to fluctuate from ~ $5{\cdot}10^5$ to $>10^6$, while the force noise in this bath drives the NR mode temperature to varying levels up to 7 times the fridge temperature. The nature of the fluctuating force noise is unclear. Careful testing indicated that it is not due to noise or thermal heating entering via signal lines or thermal loading of the sample.

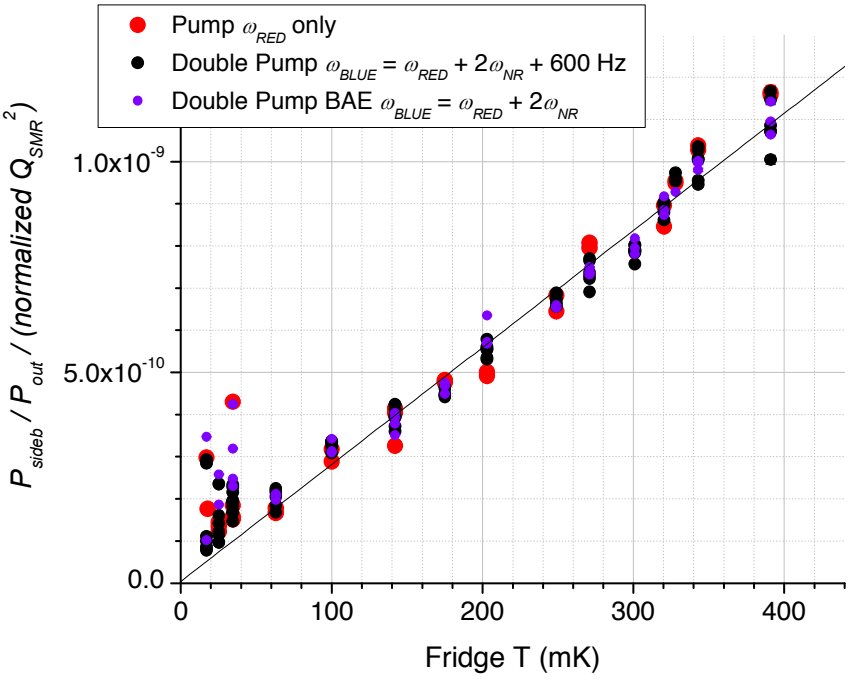

Figure SI-09. Thermal calibration data. Sideband power divided by transmitted pump power, plotted vs fridge temperature.

At temperatures above 60 mK however, coupling of the NR to this fluctuating bath was much less strong. In this regime the response to all pump configurations closely follows the fridge temperature and the measured power agrees closely with what we expect from the device. In this regime a linear regression fit of all P_{sideb}/P_{out} measurements vs fridge temperature yields

$$P_{sideb}/P_{out} = (4.20 \pm 8.79) \times 10^{-12} + (2.78 \pm 0.03) \times 10^{-9} \cdot T_m \qquad (6)$$

From this we see that the intercept is consistent with zero, and we define the empirical calibration factor $\mathrm{cal}(P_{out}) = (2.78 \pm 0.03) \times 10^{-9}$ kelvin^{-1}. (A similar analysis was also

DOI: 10.1038/NPHYS1479

done for P_{sideb}/P_{in}, yielding $\mathrm{cal}(P_{in}) = (8.33 \pm 0.05) \times 10^{-12}$ kelvin^{-1}. In the fit of P_{sideb}/P_{in} vs fridge temperature, due to excess scatter and variations in line loss or gain it was necessary to set the intercept to zero.)

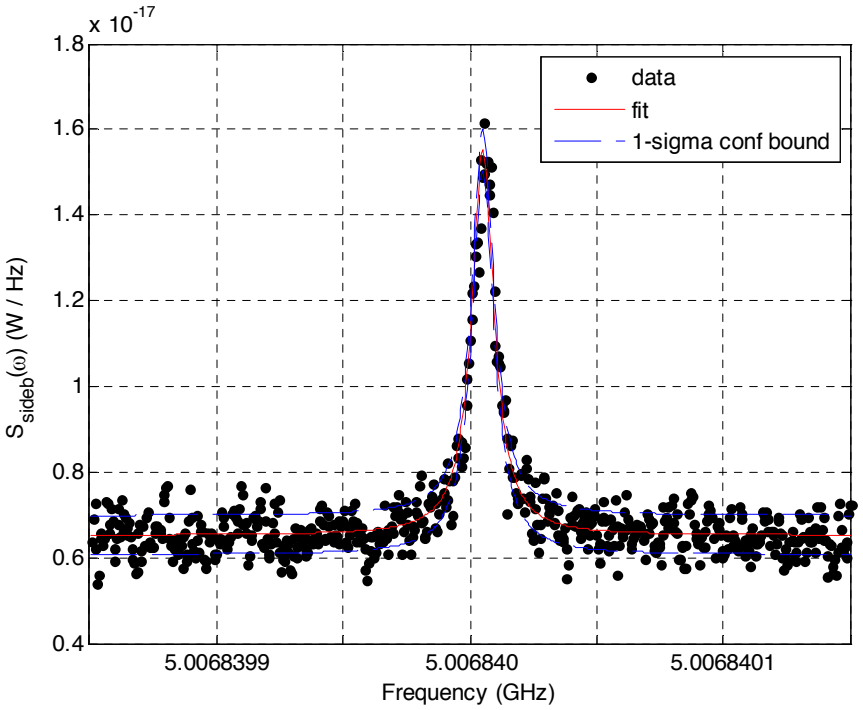

Figure SI-10. Typical motional sideband observed at frequency ω_{sr} while pumping at ω_{sr} - ω_m. Fridge T = 63 mK. Lorentzian fit yields $\Gamma_m/2\pi$ =10.4 ± 0.2 Hz, P_{sideb} = 149 ± 3 aW and S_{bgd} = 6.56 ± 0.01 aW/Hz.

Using equation (5) and the value of $\mathrm{cal}(P_{out})$, and accounting for small differences in gain at ω_{pump} and ω_{sr}, we can calculate $\partial\omega_{sr}/\partial x$. We find that $\partial\omega_{sr}/\partial x = 2\pi \times (7.5 \pm 1.6\ \mathrm{kHz/nm})$. We can also use this to make an estimate of the

capacitance C_g between NR and SR: $\partial C_g / \partial x = 3.0 \pm 0.6$ aF/nm, from which we estimate $C_g = 253 \pm 54$ aF. Capacitance of these complicated structures is difficult to estimate accurately from geometry, but our values are consistent with our experience with other samples reported elsewhere **[8]**. Thus the couplings found from device geometry, thermal calibration and backaction cooling (see section 6) all agree within reasonable bounds.

6) Backaction Cooling – Experiment vs Theory

Following **[14]**, when we pump with a single microwave tone $\omega = \omega_{sr} \pm \omega_m$, we expect backaction damping to be proportional to $\bar{n}_p$, the number of photons in the SR due to the coherent pump. In the sideband-resolved limit, the backaction damping rate Γ_{opt} is positive for $\omega = \omega_{red} = \omega_{sr} - \omega_m$, negative for $\omega = \omega_{blue} = \omega_{sr} + \omega_m$, and given by:

$$\Gamma_{opt} = \pm 4 \left(x_{ZP} \frac{\partial \omega_{sr}}{\partial x} \right)^2 \frac{1}{\kappa} \bar{n}_p \qquad (7)$$

The NR coupled in this way to the microwave mode will then achieve a mode temperature $T_m = \frac{\hbar \omega_m}{k_B} \bar{n}_m$ (assuming $\bar{n}_m >> 1$), with

$$\bar{n}_m = \frac{\Gamma_{opt} \bar{n}_m^O + \Gamma_m \bar{n}_m^T}{\Gamma_{opt} + \Gamma_m} \qquad (8)$$

DOI: 10.1038/NPHYS1479

Here, Γ_m is the intrinsic damping rate of the NR, $\bar{n}_m^T$ is the number of oscillator quanta corresponding to the temperature of the thermal bath (i.e. the fridge temperature), and $\bar{n}_m^O$ is the number of quanta corresponding to the effective backaction temperature **[14]**. In the following we will assume that $\bar{n}_m^O = 0$.

By equation (7), we expect the backaction damping and cooling to depend on the occupation of pump photons in the SR, $\bar{n}_p$. We determine $\bar{n}_p$ from either P_{in} or P_{out} using equation (3). This requires an estimate of the parameters *loss*, *gain*, and κ_{ext}. We do this as follows. By comparing the background noise level measured at the spectrum analyzer to an assumed white noise at the input of the HEMT amplifier (equal to the amplifier's specified noise temperature of 3.56 +/-1 K), and by estimating the loss in the microstrip thermalizers and circulators between the device and amplifier, we estimate that the total *gain* was ~49 dB. We observed differences of ~1 dB between gains at ω_{red}, ω_{blue} and ω_{sr}, and account for these in estimating $\bar{n}_p$. The coupling κ_{ext} of the SR to the signal lines is found by employing the mechanical sideband as a calibrated power source during backaction cooling measurements. We expect the total rate of photons $\bar{n}_m\Gamma_{opt}$ upconverted from the NR into the SR, multiplied by the SR energy per photon, to be the power in the sideband. The total measured sideband power should then be the portion of this that is emitted by the end-coupling of SR and amplified: Thus $P_{sideb} = \hbar\omega_{sr}\bar{n}_m\Gamma_{opt}\left(\kappa_{ext}/2\kappa\right)\cdot\text{gain}$. Using values of Γ_{opt} found from Lorentzian fits of the sidebands, T_m found from the sideband areas scaled by the thermal calibration, and $\bar{n}_m$ found from $T_m k_B = \hbar\omega_m\bar{n}_m$, we find that $\kappa_{ext}/\kappa = 0.61 \pm 0.24$. Using these values and

equation (2) we may determine the total input loss of the system as ~44 dB. Further discussion of these measurements appears in reference **[4]**.

With these parameters in hand, we can use equation (3) to calculate the number of pump photons $\bar{n}_p$ from measured values of P_{in} or P_{out}. We then plot the measured NR linewidth and occupation $\bar{n}_m$ against $\bar{n}_p$, as in figure 2a and 2b of the paper. The data may then be fit to the theory represented by equations (7) and (8). The measured NR linewidth $\Gamma_{tot}/2\pi$ is fit to the equation $\Gamma_{tot} = \left(\Gamma_m + \Gamma_{opt}\right) = \left(\Gamma_m + \beta \cdot \bar{n}_p\right)$, while the NR occupation $\bar{n}_m$ is fit to $\bar{n}_m = \Gamma_m \bar{n}_m^T / \left(\Gamma_m + \beta \cdot \bar{n}_p\right)$ in a simultaneous least-squares fit, using free fit parameters Γ_m, $\bar{n}_m^T$ and β. From equation (7) we note that parameter β represents the coupling between SR and NR: $\beta = (4/\kappa)\left(x_{ZP}\, \partial\omega_{SMR}/\partial x\right)^2$. Values of Γ_m and $\bar{n}_m^T$ are set by the environment and may vary from one dataset to another, but the coupling should be a fixed parameter of the device. Independent fits of several datasets found values of β agreeing within uncertainty, and we used the average of these, $\beta = 2\pi \cdot \left(3.49 \cdot 10^{-7}\ \text{Hz}\right)$, in figure 2 of the paper to produce all of the fit lines. Given that the datasets were taken on different occasions separated by weeks, these results represent reasonable fits to equations (7) and (8) using parameters that are well within expectation. The other fit parameters were

Red pump, fridge T = 142 mK: $\bar{n}_m^T = \left(752 \pm 41\right)$ and $\Gamma_m = 2\pi \times \left(19.1 \pm 3.7\ \text{Hz}\right)$

Blue pump, fridge T = 142 mK: $\bar{n}_m^T = \left(777 \pm 39\right)$ and $\Gamma_m = 2\pi \times \left(18.5 \pm 0.3\ \text{Hz}\right)$

DOI: 10.1038/NPHYS1479

From the values of the fit parameter β, and the estimated values of x_{zp} and measured value of κ, we can derive values of the coupling $\partial\omega_{SMR}/\partial x = 2\pi \times (8.0 \pm 2.1\,\mathrm{kHz/nm})$. This agrees well within uncertainty to the value derived from the temperature calibration (See section 5).

7) Position and Force Uncertainty

To calculate the position uncertainty and compare it to quantum limits, we follow conventions presented elsewhere **[1, 9, 10]**, assuming the sideband-resolved limit and that the SR is pumped at $\omega_{sr} \pm \omega_m$. We assume that no phase noise or injected noise is present in the SR, and that shot noise does not dominate. The total measured noise spectral density at frequencies near the SR resonance should be the sum of two contributions: the noise due to the mechanical sideband, $S_{sideb}(\omega)$, and a fixed-amplitude, frequency-independent background noise S_{bgd}. In principle S_{bgd} will include contributions due to both additive noise in the amplifier and vacuum fluctuations in the SR, but in our experiments the amplifier noise dominates enough to neglect the vacuum contribution.

$$S(\omega) = S_{sideb}(\omega) + S_{bgd} \tag{9}$$

The thermal calibrations and expressions for P_{sideb}, equations (4) and (6), allow us to readily calculate the position noise spectral density (in units of m^2/Hz) of the measured NR amplitude. **[7]** We use the constant $\mathrm{cal}(P_{out})$ determined from our thermal calibration

data (see section 5) to relate measured power to mechanical amplitude. (Note that we use throughout this work a convention of single-sided spectral densities.)

$$S_x^{NR}(\omega) = \left(k_B/k\right)\left(S_{sideb}(\omega)/P_{out}\right)/\mathrm{cal}(P_{out}) \tag{10}$$

The additive amplifier noise S_{bgd} contributes an uncertainty to our measurement of the NR position, expressed as a position noise spectral density S_x (in units of m^2/Hz):

$$S_x = \left(k_B/k\right)\left(S_{bgd}/P_{out}\right)/\mathrm{cal}(P_{out}) \tag{11}$$

Keeping in mind that in our measurements S_{bgd} and therefore S_x are limited by the additive amplifier noise, we can calculate the position uncertainty Δx in our measurement of the motion. This method of determining position uncertainty is equivalent to comparing additive noise with the mechanical response amplitude, as described in **[10]**. For a NR having linewidth $\Gamma_{tot}/2\pi$, this is given by the total position noise attributable to S_x within the effective noise bandwidth of the NR:

$$\Delta x = \sqrt{S_x \cdot \Gamma_{tot}/4} \tag{12}$$

We note that this procedure for determining position sensitivity may be used either for determining Δx in a non-BAE measurement or ΔX_1 in a double-pump BAE measurement. We also note that this procedure is equivalent to expressing the position uncertainty in terms of the ratio of noise floor to peak noise density, $\Delta x = \sqrt{\frac{k_B T_m}{m\omega_m^2}\frac{S_{bgd}}{S_{sideb}(\omega_{sr})}}$. When computing the ratio $\frac{\Delta x}{x_{zp}}$, we note that the effective mass

DOI: 10.1038/NPHYS1479

m drops out of the result. Thus the ratio $\frac{\Delta x}{x_{zp}}$ is independent of m, a parameter which is difficult to determine experimentally with good precision.

In general, additive amplifier noise places no fundamental limits on the uncertainty of a linear position measurement. Instead, at sufficiently high pump powers, quantum backaction should limit the sensitivity by driving the mechanical motion. (We will refer to such a condition as the shot-noise limit.) However, it is interesting to note that in the particular case of driving with only a red pump, the force noise associated with the quantum back-action corresponds to a near-zero-temperature bath: the back-action force noise does not heat the oscillator. Instead, in the limit of an infinitely strong coupling strength or cavity drive, the position uncertainty asymptotically approaches a limit set by S_{bgd}. For the ideal case of a dissipationless SR in the ideal good-cavity limit, with no losses between SR and amplifier, the position uncertainty is given by $\Delta x = \sqrt{n_{amp} + n_{vac}} \cdot \Delta x_{ZP}$, where n_{amp} is the additive amplifier noise, expressed as a number of SR quanta, and n_{vac} is the noise due to vacuum fluctuations. Because the lowest possible n_{amp} equals ½ for a quantum-limited amplifier, and n_{vac} is at least ½, the position sensitivity attained using a single red pump reaches the standard quantum limit only in the ideal case in the limit of strong coupling. Further examples of being able to reach the quantum limit in this regime are discussed in reference **[10]**. In the red-pump data presented in figure 3 of the paper, such asymptotic behavior is evident, but the limit is much greater than the ideal because of the classical noise added by our amplifier.

Because our measurements are not in the shot noise limit, and we use a filter cavity to prevent the phase noise of our microwave sources from exciting the SR, S_x is limited only by the additive noise from our microwave amplifier (T_N = 3.56 K). Using equations (11) and (12) to calculate Δx, we find that the narrow linewidths possible in the high-stress SiN nanoresonator enable Δx to approach x_{zp} at high pump powers. When two pumps at ω_{sr} +/- ω_m are applied simultaneously, parametric amplification yields further linewidth narrowing. Because small fluctuations in ω_m cause large variations in the parametric amplification, and a slight increase in the parametric amplification could cause the NR to self-oscillate, this mechanical preamplification was challenging to control. However, linewidths below 3 Hz were readily achievable and as low as 2.1 Hz were possible. In a measurement at SR occupation $\bar{n}_p \sim 1.2\times10^8$, we found $\Gamma_{tot}/2\pi$ = 2.1 Hz, reaching our lowest value of position uncertainty Δx, derived from additive amplifier noise to be $\Delta x = 1.3 \cdot x_{zp}$. The parametrically-amplified thermal noise spectrum of this measurement appears in the inset of figure 3 of the paper.

The Heisenberg uncertainty principle sets limits on the product of the measurement precision S_x, and back-action force noise S_F. For single-sided noise spectral densities, the limit is $S_x S_F \geq \hbar^2$ **[9]**. Because the NR is thermally excited to average occupations > 500 quanta, and probed at pump powers barely reaching the shot noise limit, the back-action force noise S_F is negligible, because it is incapable of driving the NR to amplitudes much exceeding one quantum of energy. Moreover, in the red-pump case, as discussed above, the back-action should always correspond to a near-zero-temperature bath. In practice, however, thermal heating or other classical mechanisms may produce a classical

DOI: 10.1038/NPHYS1479

backaction force. We have been able to establish limits on such classical back-action force, (using a dataset that is not shown in the paper) and find a limit $\sqrt{S_x S_F} \leq 90\hbar$ **[4]**.

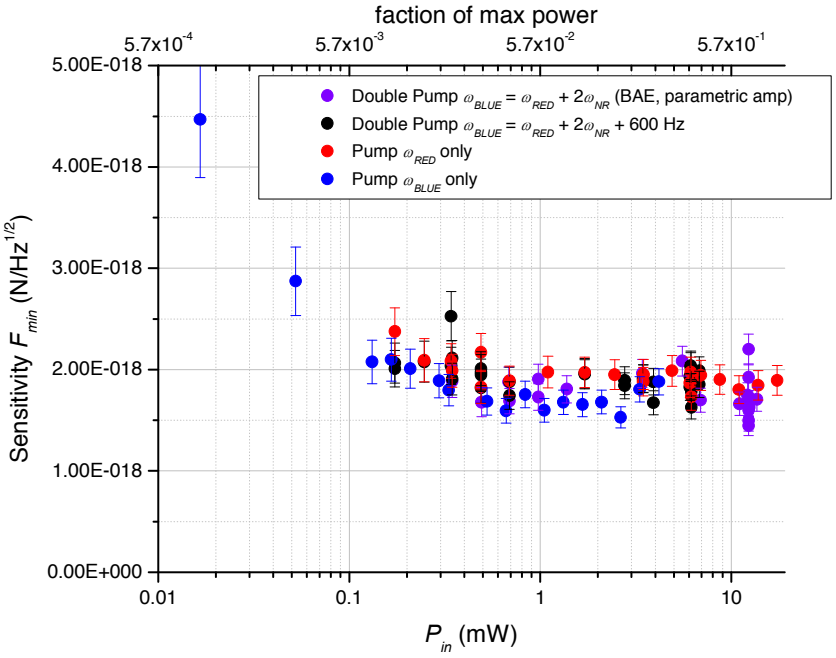

Figure SI-11. Force sensitivity at fridge temperature of 142 mK. Same dataset as in fig 2 and 3 of paper.

We can also determine the force sensitivity of the device **[11]**. For a resonator of mechanical linewidth Γ_{tot}, the force sensitivity F_{min} represents the minimum force per unit bandwidth which would produce a mechanical signal that is detectable above the spectral density S_x of position uncertainty and the thermally-excited amplitude of the NR. It is given (in units of $\mathrm{N}/\sqrt{\mathrm{Hz}}$) by

$$F_{\min} = m\omega_m \Gamma_{tot} \sqrt{S_x + 4\frac{k_B T_m}{m\omega_m^2 \Gamma_{tot}}} \qquad (13)$$

Figure SI-11 shows the force sensitivity F_{min} calculated for measurements at a temperature of 142 mK (fig 2 & 3 in the paper). At high pump powers, we have sufficient sensitivity that in equation (13) the thermal noise of the NR dominates over S_x. At this temperature we reliably achieve a force sensitivity of $1.7 \cdot 10^{-18}\, N/\sqrt{Hz}$. Figure SI-12 shows force sensitivity vs fridge temperature, for the same dataset used in our thermal calibration (figure SI-09). At the lowest temperature at which the sample thermalized to the fridge (63 mK), we reliably achieved sensitivity of $8 \cdot 10^{-19}\, N/\sqrt{Hz}$ at high pump powers. At our lowest fridge temperature of ~17mK, we occasionally observed a NR mode temperature of 46mK and linewidth of 8 Hz, yielding a force sensitivity of $6 \cdot 10^{-19}\, N/\sqrt{Hz}$.

By examining the data in the thermal calibration measurement (section 5) we may also estimate the force noise which dominates the NR behavior at fridge temperatures below 60 mK. At these temperatures the NR has linewidths of 5 to 10 Hz and has apparent mode temperatures of ~50 to ~150 mK, indicating that it is excited by a force noise of $3 \cdot 10^{-19}$ to $10^{-18}\, N/\sqrt{Hz}$. This force noise fluctuates unpredictably in magnitude. The effect of microwave pump power on this noise is unclear.

DOI: 10.1038/NPHYS1479

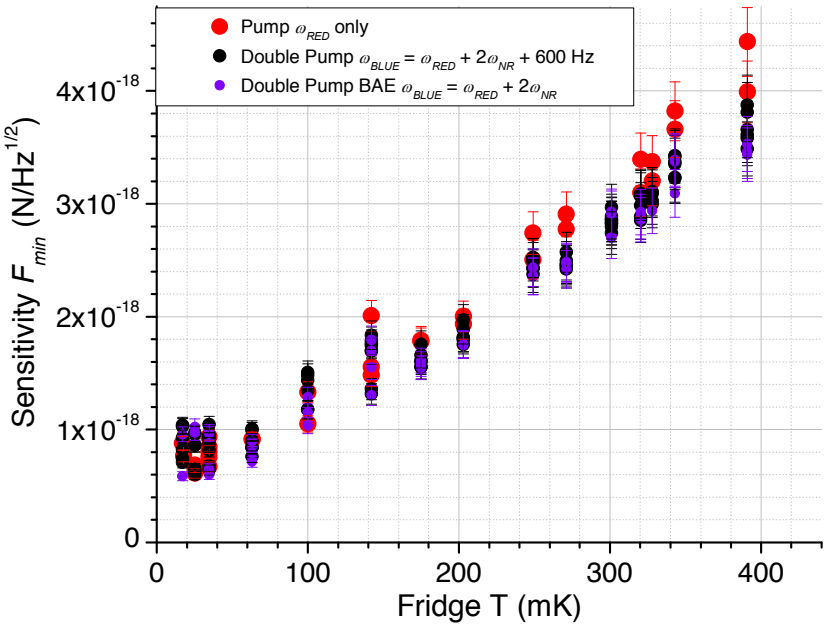

Figure SI-12. Force sensitivity vs fridge temperature. Same dataset as thermal calibration (fig SI-09).

8) Technique for Backaction Evasion

Backaction evasion requires the application of pump signals of equal strength (power circulating within the SR) at frequencies $\omega_{sr} \pm \omega_m$. Methods of equalizing pump strength are discussed in reference **[4]**. Noise was injected into the SR at frequencies around ω_{sr}, to drive the NR with backaction and demonstrate backaction evasion (BAE). Drifts of a few Hz in ω_m required readjustment of the blue pump, limiting our averaging time. After averaging the spectrum centered on ω_{sr} for ~1 hour, we shut off the blue pump to observe

the backaction-driven motion. The backaction produced when driving with a single tone is expected and found to drive both quadratures (X_1 and X_2) equally. The backaction-driven single-pump and backaction-evading double-pump spectra appear in figure 4 of the paper and in figure SI-13. The measurements were made at weak enough pump powers that we may neglect parametric amplification in the BAE measurement.

Determination of the BAE efficiency $\left\langle X_1^2 \right\rangle / \left\langle X_2^2 \right\rangle$ requires knowledge of the amplitudes of motion in the two quadratures when performing backaction evasion. Because the X_2 quadrature is not directly observable during BAE measurement, we estimate its amplitude based on the separate measurement of backaction using a single red-detuned pump and the same level of injected noise at frequencies around ω_{sr}.

We consider the situation in which the SR is excited out of its ground state by noise. We let $\bar{n}_{sr}^T$ represent the number of SR photons due to this additional noise. When $\bar{n}_{sr}^T > 0$, the backaction will no longer appear as a zero-temperature bath to the NR. In the sideband resolved limit, a theoretical calculation along the lines of Ref **[14]** which includes cavity noise finds that Eq. (7) remains valid, but that the effective back-action temperature $\bar{n}_m^O = \bar{n}_{sr}^T$. The occupation $\bar{n}_{sr}^T$ may be calculated from the measured white noise spectrum at ω_{sr} by first subtracting the portion attributable to amplifier noise, and scaling the result by the system gain to find the noise spectral density $S_{out}(\omega_{sr})$ emitted by the SR at resonance. We then find $\bar{n}_{sr}^T = (\kappa/2\kappa_{ext})(1/\hbar\omega_{sr}) \cdot S_{out}(\omega_{sr})$. Note that we treat $\bar{n}_{sr}^T$ as thermal noise associated with the cavity dissipation. However, recent theoretical

DOI: 10.1038/NPHYS1479

work looking at the effects of pump phase noise **[12]** shows that one may also model phase noise as an effective thermal noise in the relevant limit $\Gamma_{opt} << \kappa$ and $\omega_m >> \kappa$.

The back-action driving of the NR due to the SR excitation will produce a sideband signal at ω_{sr} that is coherent with but 180 degrees out of phase with the SR noise at ω_{sr}. Therefore the sideband signal due to backaction subtracts from the SR noise at ω_{sr}. A careful theoretical calculation shows that the area of this sideband, expressed as an effective NR occupation $\bar{n}_m^{eff}$, is given by

$$\bar{n}_m^{eff} = \frac{\Gamma_m}{\Gamma_{opt}+\Gamma_m}\bar{n}_m^T - \left(1+\frac{\Gamma_m}{\Gamma_{opt}+\Gamma_m}\right)\bar{n}_{sr}^T \qquad (14)$$

Here the term $\left(\Gamma_m/\left(\Gamma_{opt}+\Gamma_m\right)\right)\bar{n}_m^T$ represents the NR thermal noise while the term $-\left(1+\left(\Gamma_m/\left(\Gamma_{opt}+\Gamma_m\right)\right)\right)\bar{n}_{sr}^T$ represents the backaction signal subtracting coherently from the SR noise. If the latter dominates, then the sideband will appear as a "dip" in the SR noise rather than a peak. We determine $\bar{n}_m^{eff}$ from the sideband area by using the thermal calibration (exactly as in the case where $\bar{n}_{sr}^T = 0$). Taking the sideband-resolved limit where $\bar{n}_m^O = \bar{n}_{sr}^T$ we may then use equation (8) to calculate how much the SR excitation increases $\bar{n}_m$. In terms of the measured quantities $\bar{n}_m^{eff}$ and $\bar{n}_{sr}^T$ we find

$$\bar{n}_m = \bar{n}_m^{eff} + 2\bar{n}_{sr}^T \qquad (15)$$

In the BAE demonstration, we use strong enough noise to excite the SR via backaction into a thermal state with occupation factor $\bar{n}_{sr}^T > 10^4$. At the measurement temperature of

142 mK, backaction driving therefore dominates the motion of the NR and we may neglect thermally-driven motion. Assuming the "good cavity" limit $\omega_m / \kappa >> 1$, we can use standard input-output theory to calculate the output spectrum of the SR when driven by noise at ω_{sr} and a single pump tone at $\omega_{sr} - \omega_m$. The spectrum should consist of a negative Lorentzian peak representing backaction-driven NR motion out of phase with the noise at the SR resonance. This is exactly what we observe. We fit the peak area to find sideband power $P_{BA,red}$ and linewidth $\Gamma_{tot} = \Gamma_m + \Gamma_{opt}$.

In the BAE measurement, no motional sideband is distinguishable in the noise spectrum at ω_{sr}. As described in **[13]**, deviation from the "good cavity" ideal does enable noise at $\omega_{sr} \pm 2\omega_m$ to drive the NR via backaction. If we could average the noise spectrum indefinitely, we would expect to resolve a lorentzian peak representing this motion. Instead, we estimate the maximum possible sideband amplitude consistent with the random noise observed at ω_{sr}. We take this to be the standard error of the measured noise power density within the noise bandwidth $\Gamma_m/4$ of the NR. Multiplying this by the noise bandwidth $\Gamma_m/4$ yields an estimate of the minimum resolvable sideband power in the BAE measurement, denoted as P_{BAE}.

DOI: 10.1038/NPHYS1479

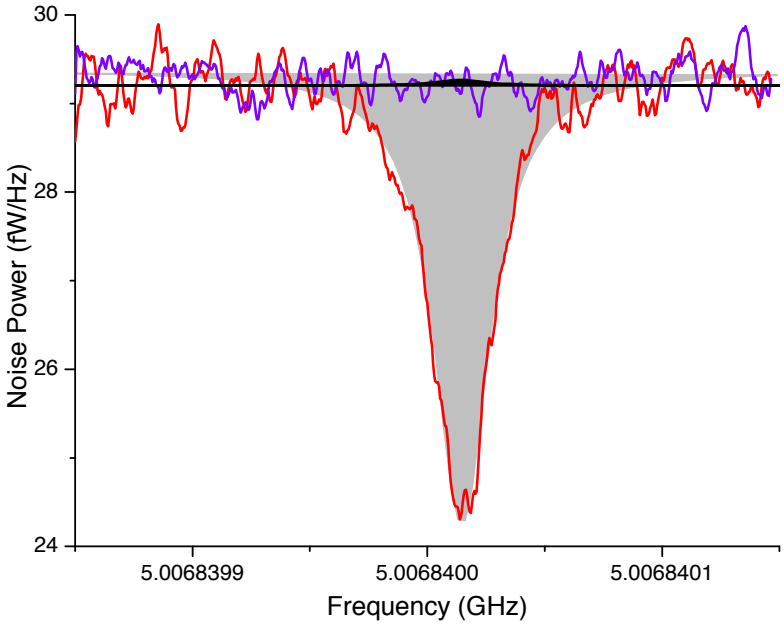

Figure SI-13. Data from fig 4 of the paper. Red line is motional sideband observed while pumping at ω_{red} and injecting noise to the SR. Lorentzian fit (gray shaded area) yields linewidth $\Gamma_{tot} = 2\pi \times (29 \pm 0.5)$ Hz and $P_{BA,red}$ = -234 ± 3 fW. Purple line is measured BAE noise spectrum. Black shaded area is a Lorentzian with amplitude equal to standard error of measured noise within span $\Gamma_{nr}/4 = (\pi/2) \times (24.2 \pm 0.8)$ Hz. Area of this region is P_{BAE} = 2.46 fW, representing the maximum possible sideband power consistent with the measured noise.

To estimate $\langle X_1^2 \rangle / \langle X_2^2 \rangle$ from our measured values of P_{BAE} and $P_{BA,red}$, we compare our calculation for the single-pump case with the calculations presented in **[13]** for BAE X_2 amplitude, applied to large classical noise occupation $\bar{n}_{sr}^T$ in the SR. We find

$$\frac{\left\langle X_1^2 \right\rangle}{\left\langle X_2^2 \right\rangle} = \left[8 \frac{\Gamma_{opt}}{\Gamma_{NR}} \frac{\Gamma_{tot}}{\Gamma_{tot} + \Gamma_{NR}} \frac{\left| P_{BA,red} \right|}{P_{BAE}} \right]^{-1} \qquad (16)$$

This result employs the definition of optical damping presented in **[14]**, and accounts for the different damping in the single-pump vs BAE cases and for the fact that total pump power in the BAE case is double that in the single-pump case. For measured values $P_{BA,red}$ = -234 fW, P_{BAE} = 2.46 fW, $\Gamma_{nr} = 2\pi \times 24$ Hz and $\Gamma_{tot} = 2\pi \times 29$ Hz , equation (16) yields $\left\langle X_1^2 \right\rangle / \left\langle X_2^2 \right\rangle = 1.2 \times 10^{-2}$. This represents an upper bound on the effectiveness of our backaction evading measurement, limited by averaging duration.

9) Parametric Amplification and Instability

Parametric amplification effects are relevant to the backaction-evading measurements. Figure SI-14 shows a measurement of the NR frequency while driving with a red pump at frequencies detuned from the optimum value of (ω_{SR} - ω_m). The NR exhibits an optomechanical frequency shift, as described in **[14]**. This shift is combined with an electrostatic shift, proportional to the mean square voltage in the SR, corresponding to an electrostatic spring constant $k_e = -(\partial F / \partial x) = \frac{1}{2}\left(\partial^2 C_g / \partial x^2\right)\left\langle V^2 \right\rangle$. When double pumps are applied in BAE configuration, the electrostatic spring constant oscillates at $2\omega_m$, leading to parametric amplification of the NR motion.

From the fit line in the plot, we can derive $\partial^2 C_g / \partial x^2 = 0.06$ F/m^2, which is in reasonable agreement with other estimates of C_g and with the approximation $\partial^2 C_g / \partial x^2 = C_g / d^2$.

DOI: 10.1038/NPHYS1479

From this we may estimate $\lambda = (\omega_{sr}/2C)(\partial^2 C_g/\partial x^2) = 2\pi \cdot 0.15\,\mathrm{kHz/nm^2}$. We may also estimate the shift in NR resonance frequency $\Delta\omega = \frac{1}{2}\omega_m k_e/k$, which oscillates along with k_e. For $\Delta\omega \geq \Gamma_m$, we expect the NR to become unstable and self-oscillate. At the pump powers at which we made our highest BAE measurements, cavity occupation was $\bar{n}_p = 1.1 \cdot 10^8$, for which we estimate a parametric NR frequency shift $\Delta\omega \approx 2\pi \cdot 9\,\mathrm{Hz}$. This approaches the measured linewidth of Γ_m = 15 to 20 Hz, agreeing with the observation that at somewhat higher powers the parametric amplification becomes severe and leads to self-oscillation. Further details of this measurement and calculation appear in reference **[4].**

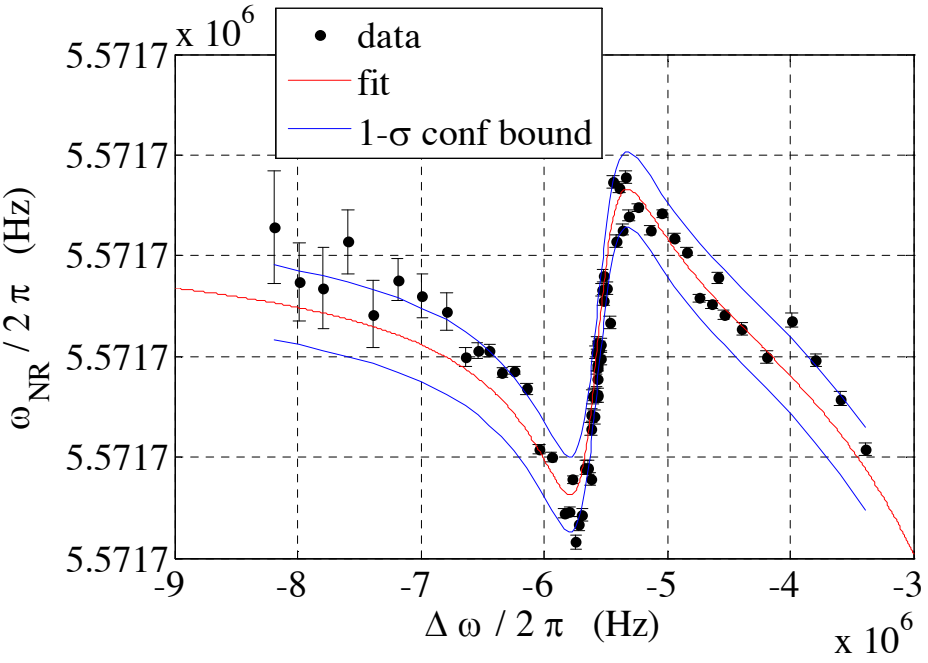

Figure SI-14. NR frequency shift vs pump detuning, with fit of combined optomechanical and electrostatic shift.

References

[1] LaHaye, M. "The Radio-frequency single-electron transistor displacement detector." Ph.D. dissertation, University of Maryland, College Park, 2005.

[2] Biquard, F and Septier, A. Improvement of the surface conductivity of copper and aluminium at hyper-frequencies by lowering the temperature. *Nuclear Instr and Methods* **44** (1) 18-28 (1966).

[3] Rogers, R. G., *Low Phase Noise Microwave Oscillator Design*, (Artech House, 1991).

[4] Jared B. Hertzberg. Back-action evading measurements of nanomechanical motion approaching quantum limits. PhD thesis, University of Maryland, College Park, 2009.

[5] Frunzio, L., Wallraff, A., Schuster, D., Majer, J. and Schoelkopf, R. Fabrication and characterization of superconducting circuit QED devices for quantum computation. *IEEE Trans Appl Supercon* **15** (2) 860-863 (2005).

[6] Pozar, David. *Microwave Engineering*, (John Wiley, 2005).

[7] LaHaye, M. D., Buu, O., Camarota, B., Schwab, K.C., Approaching the Quantum Limit of a Nanomechanical Resonator. *Science* **304**, 74-77 (2004).

[8] Naik, A., Buu, O., LaHaye, M.D., Armour, A.D., Clerk, A.A., Blencowe, M.P., Schwab, K.C., Cooling a nanomechanical resonator with quantum back-action. *Nature* **443**, 193-196 (2006).

[9] Braginsky, Vladimir B., Khalili, Farid YA., *Quantum Measurement*, (Cambridge University Press, Cambridge, UK, 1992), edited by Thorne, Kip S.

[10] Clerk, A. A., Devoret, M. H. Girvin, S.M., Marquardt, F., Schoelkopf, R.J. Introduction to Quantum Noise, Measurement and Amplification. arXiv:0810.4729v1 (unpublished)

[11] Mamin, H.J., Rugar, D., Sub-attonnewton force detection at millikelvin temperatures. *Appl. Phys. Lett.* **79**, 3358-3360 (2001).

[12] Rabl, P., Genes, C., Hammerer, K. and Aspelmeyer, M. Phase-noise induced limitations in resolved-sideband cavity cooling of mechanical resonators. arXiv:0903.1637v1 (unpublished).

[13] Clerk, A.A., Marquardt, Florian, Jacobs, K., Back-action evasion and squeezing of a mechanical resonator using a cavity detector. *New J. Phys.* **10**, 095010 (2008).

[14] Marquardt, Florian, Chen, Joe. P., Clerk, A.A., and Girvin, S.M., Quantum Theory of Cavity-Assisted Sideband Cooling of Mechanical Motion. *Phys. Rev. Lett.* **99**, 093902 (2007).